NuSTAR on-ground calibration I: Imaging quality

Niels J. Westergaard[a], Kristin K. Madsen[b], Nicolai F. Brejnholt[a], Jason E. Koglin[c], Finn E. Christensen[a], Michael J. Pivovaroff[d], and Julia K. Vogel[d]

[a]Technical University of Denmark, Kgs. Lyngby, Denmark;
[b]California Institute of Technology, Pasadena, CA, USA;
[c]Columbia University Astrophycs Laboratory, New York, NY, USA;
[d]Lawrence Livermore National Laboratory, Livermore, CA, USA;

ABSTRACT

The Nuclear Spectroscopic Telescope Array (NuSTAR) launched in June 2012 carries the first focusing hard X-ray (5 - 80 keV) telescope to orbit. The on-ground calibration was performed at the RaMCaF facility at Nevis, Columbia University. During the assembly of the telescopes, mechanical surface metrology provided surface maps of the reflecting surfaces. Several flight coated mirrors were brought to BNL for scattering measurements. The information from both sources is fed to a raytracing code that is tested against the on-ground calibration data. The code is subsequently used for predicting the imaging properties for X-ray sources at infinite distance.

Keywords: The NuSTAR mission, calibration, raytracing, simulation

1. INTRODUCTION

The NuSTAR[1] mission was launched in June 2012 and it carries two high energy X-ray telescopes covering the energy range 5 - 80 keV. They have been calibrated on ground in March 2011[2,3] in the Rainwater Memorial Calibration Facility (RaMCaF) at the Nevis Laboratory (N.Y.). The mirrors have been coated with multilayers[4] to obtain good reflectivity up to 80 keV. The materials for the inner 89 mirror layers are Pt and C, and W and Si for the outer 44 layers.

This contribution describes the imaging quality as expressed by the point spread function (PSF), which depends on the source position in the Field-Of-View (FOV) whereas an accompanying paper[5] focuses on the effective area based on detailed reflectivity measurements and raytracing.

The prediction of the details of the PSF is made by using a raytracing system (MT_RAYOR[6]) that includes the geometry of the optics and the detailed shape of the reflecting surfaces down to a length scale of 2 mm. The X-ray scattering is included in a statistical way based on measured distributions and modelled scattering fractions. The validation of the raytracing is sought by comparing data from the on-ground calibration in the diverging beam with the raytracing predictions.

For the detailed calibration measurements of the effective area a Ge-detector with an active surface area of 20 cm^2 shielded off by a slit system was used. This detector has a well-defined response over the entire energy range but gives no position information. Additional measurements were made with an imaging detector, a CsI(Tl) scintillator coupled to an electron multiplying CCD (EMCCD)[7] developed by RMD with an effective area of $2.5\,cm \times 2.5\,cm$. In particular these results provide detailed information on the imaging properties and the comparison with the raytracing results makes it possible to extrapolate to X-ray sources at infinite distances.

A satisfactory agreement between these measurements and the raytracing results will validate the extrapolation.

Further author information: (Send correspondence to N.J.W.)
N.J.W.: E-mail: njw@space.dtu.dk, Telephone: +45 4525 9705

Space Telescopes and Instrumentation 2012: Ultraviolet to Gamma Ray,
edited by Tadayuki Takahashi, Stephen S. Murray, Jan-Willem A. den Herder,
Proc. of SPIE Vol. 8443, 84431X · © 2012 SPIE · CCC code: 0277-786/12/$18 · doi: 10.1117/12.927076

2. CALIBRATION SETUP

The installation in RaMCaF[2,3] consists of an X-ray tube situated 163.1 m in front of the center of the NuSTAR optic. As the focal length is 10.15 m the detectores are placed 670 mm behind the nominal focal plane.

The X-ray emission spot on the X-ray tube has a dimension of 5 mm horizontally and 12 mm vertically. This is implemented in the raytracing setup by defining a set of 6×13 point sources separated by 1 mm. The angular separation is about 1 arcsec, far less than the angular resolution of the optics, so a finer mesh is not required.

During measurements the optic is mounted in such a way[3] that it can be rotated in all three directions. The aperture can be covered with a selection of plates that allow the radiation to reach one or a few subgroups of mirror layers for detailed investigations. 20 subgroups, each consisting of 6 – 8 layers, have been defined.

3. OPTICS

3.1 Structural components

The 133 mirror shells are held in place by a number of spacers so that the unsupported angular span is ∼15 degrees for the inner 68 shells and ∼7.5 degrees for the outer 65 shells. They are made of carbon fiber reinforced epoxy that spans the full range along the mirror substrate (glass). A so-called spider structure fixes the optic to the satellite structure. The six spider 'legs' are aligned with the six main spacers to minimize blocking of the beam.

In the NuSTAR flight configuration an aperture stop is placed 800 mm above the focal plane as a circular hole with a diameter of 206 mm to let the doubly reflected X-rays through and prevent stray light and radiation from sources outside the FOV to fall on the detector. This is not used in the RaMCaF setup.

3.2 Mirror shapes

During the optic assembly process where the mirrors were laid down at the rate of one layer per day, a mechanical scanning[2] along the optical axis was carried out for about 120 azimuth angles with a resolution of 0.2 mm in the axial direction (also called z-direction). Only the backside (which is not used for X-ray reflection) of the glass pieces can be scanned in this way. Nevertheless these scans can still be considered as representative of the active surface since thickness variations are expected to be very small indeed, in particular because the scans are in the same direction as the draw direction in the manufacturing process of the glass.

These results are imported to the raytracing for each layer and mirror position and is taken into account for each reflection.

3.3 Effect of gravity

The laboratory measurements are done with the optic in horizontal position suspended between the spiders in both ends. The resulting gravitational bend amounts to ∼8 microns which is included in the modelling as a parabolic shape in addition to the deformations mentioned above.

This bending was not measured mechanically but estimated from asymmetries in the central spot as it appears in the EMCCD detector measurements (see later).

4. MIRROR PROPERTIES

4.1 Multilayer surfaces

As described in the accompanying paper[5] the crucial properties, such as multilayer thicknesses and surface roughness, vary across each surface. This implies that the coefficient of reflection depends not only on photon energy and grazing angle but also on where the photon interacts with the mirror. This is handled by writing a list a photons with tags for interaction details. The file is then read into an auxiliary code that looks up the extra information available on the multilayer properties and recalculates the reflection coefficients for at more realistic evaluation of e.g. effective area.

4.2 Scattering

A series of scattering measurements on flight mirrors were made at the NSLS synchrotron of the Brookhaven National Laboratories with realistic grazing angles and three different energies representative of the NuSTAR range. The setup used was a 2-theta-scan yielding the intensity for all scattering angles up to 2-3 degrees. Due to the high beam intensity it was possible to cover 7 orders of magnitude of the reflected beam.

The selection of mirrors was made to cover the relevant angles and samples of the coating materials (Pt/C or W/Si). Figure 1 shows the resulting scattering curves for various cases aiming at isolating a single parameter (energy, material, or angle).*

In these measurements the mirror figure errors made it difficult to distinguish between the scattered component and the specularly reflected beam. Even with a rather short beam footprint on the mirror the reflected peak showed a broadening and in some cases even multiple peak features.

A theoretical framework,[8,9] further developed by one of us (MP), has allowed to determine the scattered part as a function of energy and grazing angle. The specularly reflected part is treated as a delta-function.

As can be seen from the figure 1 the shape of the scattered part does not differ in a drastic way from coating to coating type or from energy to energy. Some structure is apparent where the multi-layer effects come into play.

Raytracing tests have indicated that the PSF HPD increases from 44 arcsec to 49 arcsec when scattering is introduced on top of the LVDT figure errors. Consequently a precise modelling of the scattered part is not required to obtain a good estimate of the shape of the PSF. The collimation of the layers themselves reduces the importance of the intensity in the larger scatter angles.

5. COMPARISON WITH EMCCD DETECTOR EXPOSURES

During calibration measurements PSF data were acquired using the above mentioned EMDDC camera. In order to obtain the PSF of the entire telescope, the optics were systematically rotated about their optical axis and horizontal raster-scans were acquired at each rotation position in order to study the whole extent of the PSF with the available detector area. The images are then stitched together with appropriate weighting to compensate for exposure time and changes in the incoming beam intensity.

Figure 2 shows such a mosaic image together with the best fitting raytracing with allowance for small adjustments in yaw and pitch to compensate for small deviations from precise alignment of the optic.

Similarly the modelling of the gravitationally induced bending has been adjusted to match the vertical asymmetry in the EMCCD image, see figure 3 that shows a cross section through the peak for both the EMCCD data and the simulation. The cross sections represent a 4 mm wide belt in both the horizontal and vertical direction.

The similarity of the peak size for EMCCD and for the simulation lends credibility to the derived PSF for infinite source distance.

It must be emphasized that the response of the EMCCD detector is not a linear function of the intensity so this comparison is just a preliminary version. Work is on-going to fold the predicted beam into the detector response to get a more accurate basis for comparison.

6. ASSESSMENT OF THE IN-FLIGHT PSF

6.1 Encircled energy fraction

The calculations for this section have been done for a point source at infinite distance and the aperture stop has been included. The mechanical stress in the optics is assumed to be so small that deformations can be neglected.

The encircled energy fraction is an important parameter for the flux determination from celestial point sources. A set of these curves is shown in figure 4 from raytracings at three energies, 10, 40, and 70 keV. The contributions from surface figure errors and from scattering are show separately and combined.

*The designations N260 and N336 in the headers are substrate identifiers.

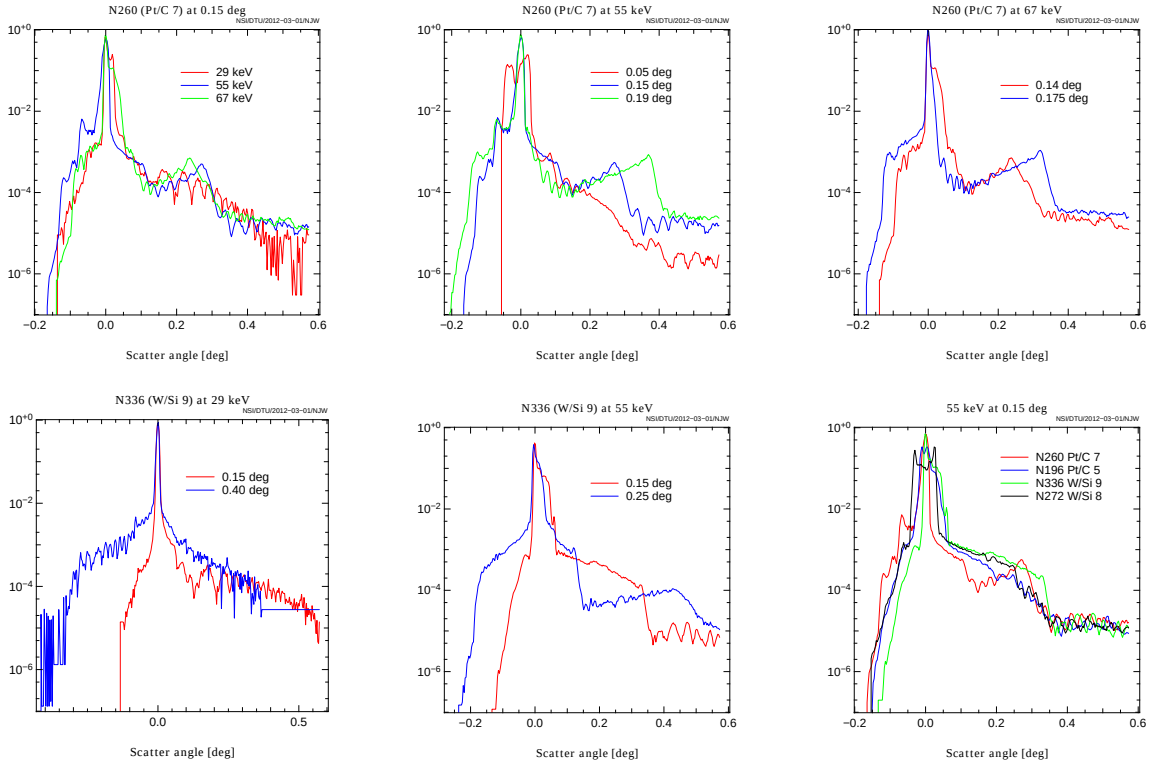

Figure 1. Reflected intensity as a function of scatter angle as measured from the specular direction normalized to 1 at the peak. *First row:* **Left panel:** Pt/C, same angle, different energies. **Mid panel:** Pt/C, same energy, different angles. **Right panel:** Pt/C, same energy, different angles. *Second row:* **Left panel:** W/Si, same energy, different angles. **Mid panel:** W/Si, same energy, different angles. **Right panel:** Same angle and energy, different coatings.

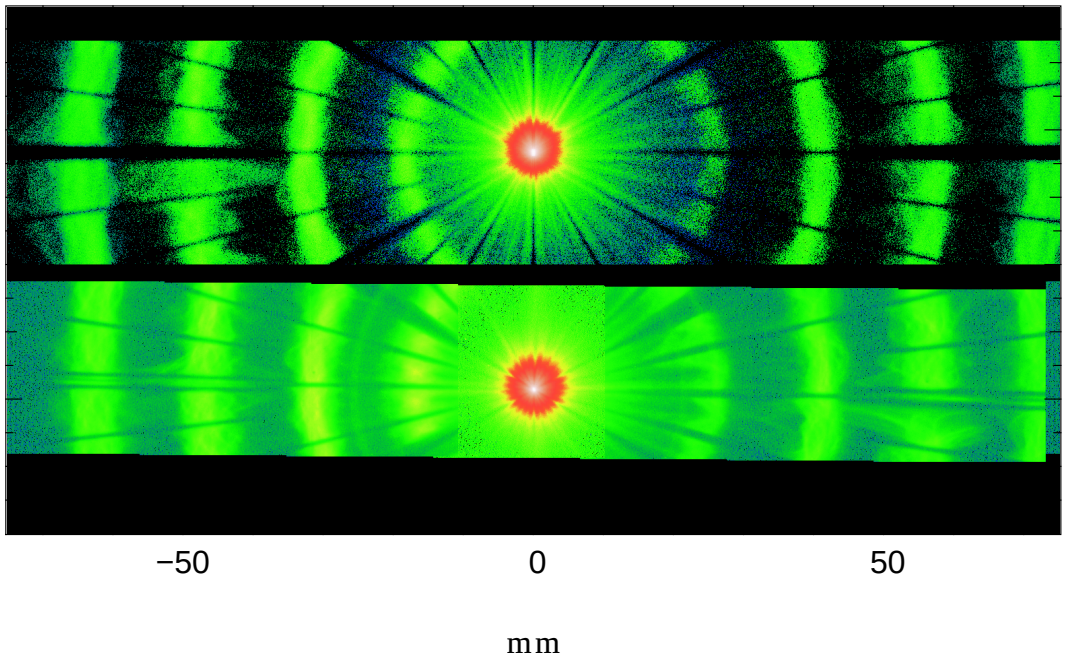

Figure 2. The EMCCD image stitched together at the bottom and the simulated image for a yaw angle of +0.67 arcmin.

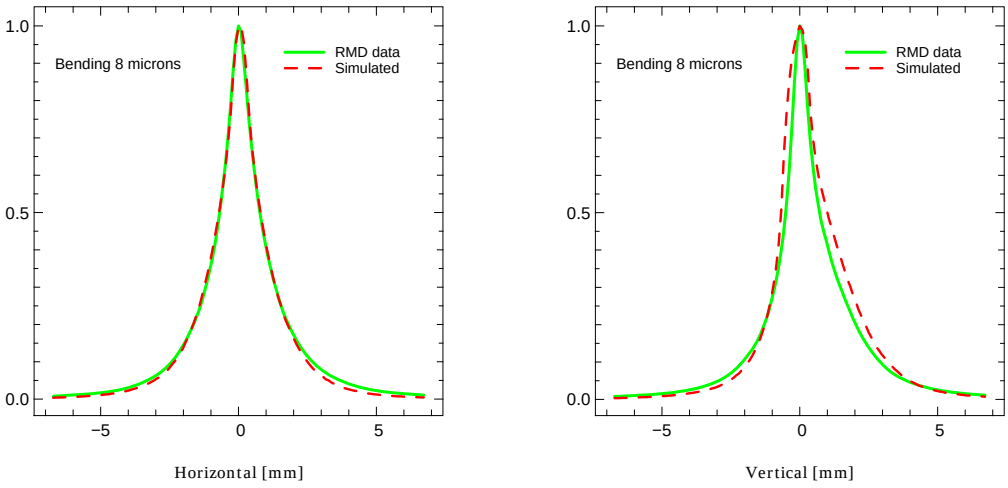

Figure 3. Comparing the cross sections in the horizontal and vertical direction. A belt of a width of 4 mm was used in both directions.

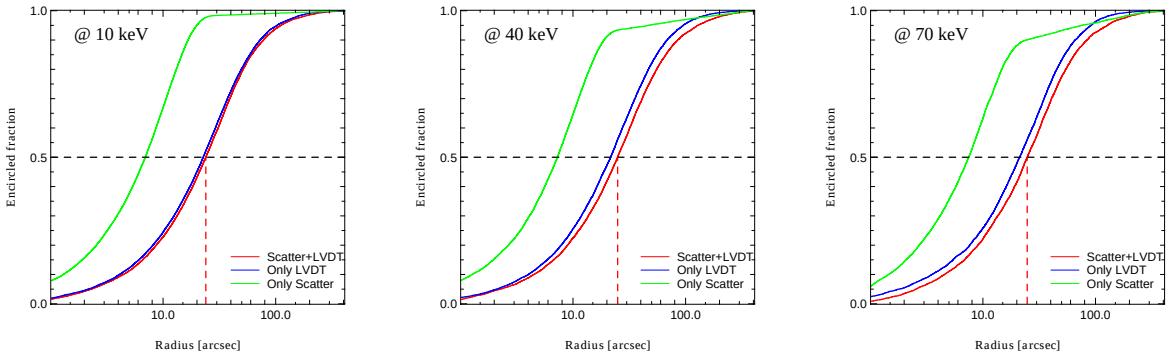

Figure 4. Curves of the encircled energy fractions showing the relative contributions of the figure errors and scattering at 10, 40, and 70 keV.

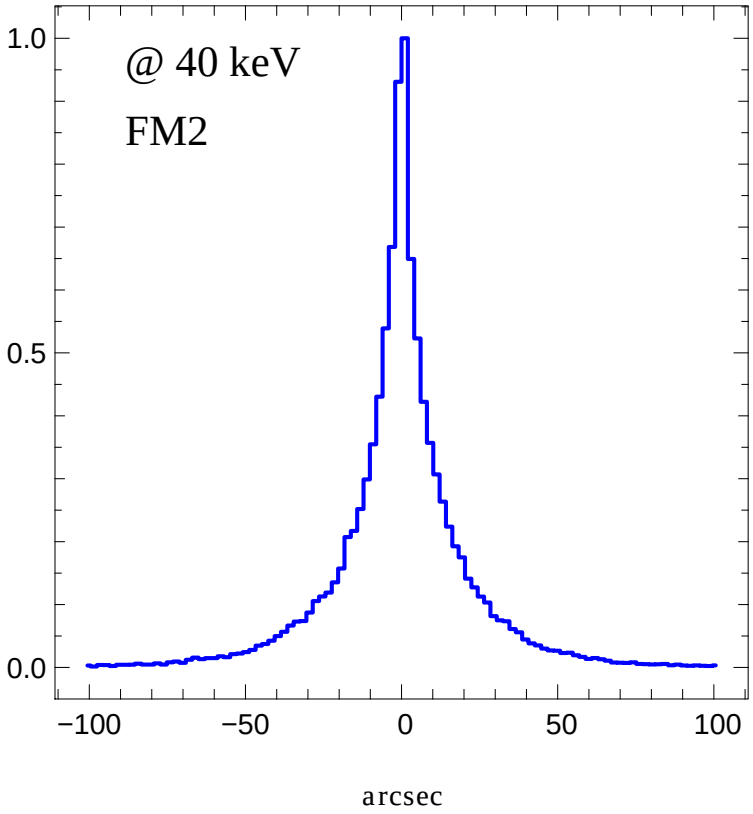

Figure 5. A slice of width 2 mm through the on-axis PSF showing the narrow peak and wider tails.

In principle the HPD value is a function of energy, but for on-axis sources this dependence is rather weak, see the right hand panel in figure 7.

Table 1 gives the numbers at three energies for both NuSTAR optics. They are about 5% smaller than the number (52 ± 4 arcsec for both optics) given by Koglin *et al.*,[2] but it should be kept in mind that the present figures depend heavily on the LVDT scan results that have been filtered to avoid spikes and edge effects in the data.

Table 1. Table of encircled fractions in arcsec

	HPD (50% width			W75 (75% width)		
	10 keV	40 keV	70 keV	10 keV	40 keV	70 keV
FM1	48	50	50	89	95	93
FM2	46	48	46	86	93	89

6.2 Shape of the PSF

The on-axis PSF is rather pointed with a FWHM of ∼13 arcsec as shown in figure 5. The figure shows a histogram of photons falling in a 2 mm wide band through the center of the peak.

6.3 Dependence on position in FOV

Figure 6 is an image of the focal plane using detector subpixels i.e. with a size that is a fifth of the physical pixel, 0.12 mm on a side or 2.4 arcsec. The flight detector is constructed from four square CdZnTe crystals with

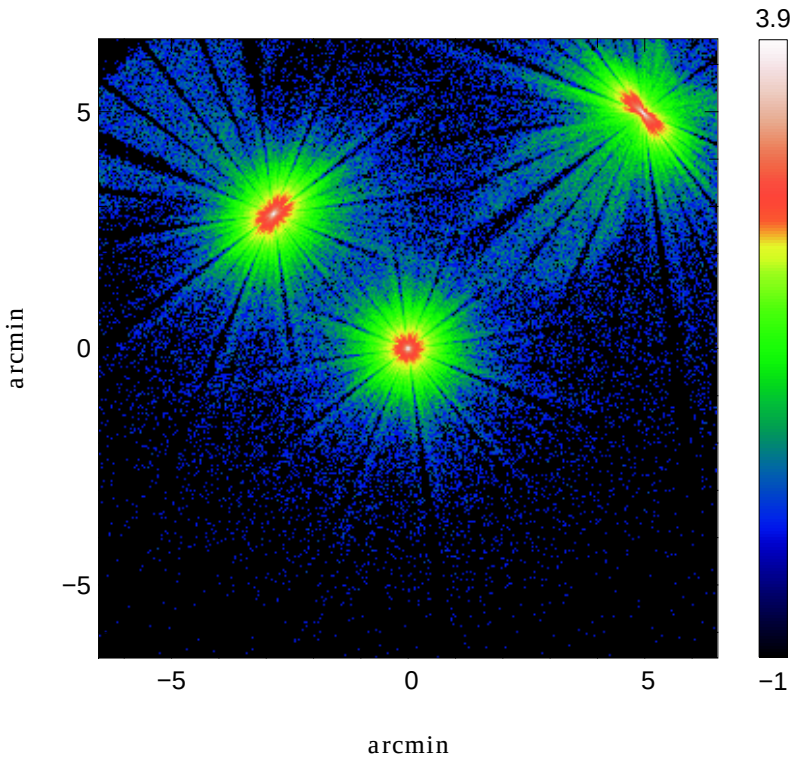

Figure 6. Three sources in the NuSTAR FOV, one on-axis and two with off-axis angles of 4 and 7 arcmin, resp. The color scale is logarithmic (the colorbar shows the logarithm (base 10) of the number of counts). This illustrates how the counts from a source are distributed over a large part of the detector.

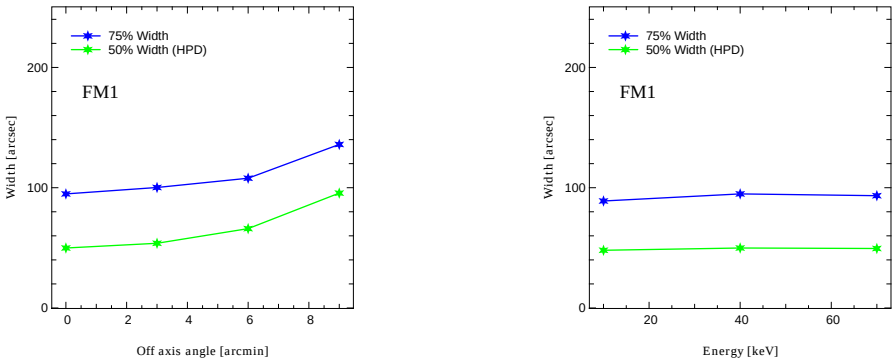

Figure 7. The 50% (HPD) and 75% widths plotted as a function of off-axis angle (left panel) and as a function of photon energy (right panel).

a small separation between them which has been neglected here. The photons from three sources are shown in a logarithmic color scale that strongly enhances the low intensity regions.

The varying shape of the PSF is apparent. In spite of this the encircled energy fraction is derived as a function of radius and is shown in figure 7. For source near the edge of the FOV it would be advantageous to use e.g. an oval shaped region to collect the counts.

7. CONCLUSION

The NuSTAR inflight calibration is on-going while these lines are being written so very soon we will be able to compare this modelling to the facts and the tools are ready.

Acknowledgements

The work was performed under the auspices of the U.S. Department of Energy by Lawrence Livermore National Laboratory under contract DE-AC52-07NA27344. The support of the Laboratory Directed Research and Development Program is gratefully acknowledged.

REFERENCES

[1] Harrison, F. A., Boggs, S., Christensen, F., Craig, W., Hailey, C., Stern, D., Zhang, W., Angelini, L., An, H., Bhalereo, V., Brejnholt, N., Cominsky, L., Cook, W. R., Doll, M., Giommi, P., Grefenstette, B., Hornstrup, A., Kaspi, V., Kim, Y., Kitaguchi, T., Koglin, J., Liebe, C. C., Madejski, G., Kruse Madsen, K., Mao, P., Meier, D., Miyasaka, H., Mori, K., Perri, M., Pivovaroff, M., Puccetti, S., Rana, V., and Zoglauer, A., "The Nuclear Spectroscopic Telescope Array (NuSTAR)," in [*Space Telescopes and Instrumentation 2010: Ultraviolet to Gamma Ray Optics*], *Proc. SPIE* **7732**, 77320S (2010).

[2] Koglin, J. E., An, H., Barrière, N., Brejnholt, N., Christensen, F. E., Craig, W. W., Hailey, C. H., Jakobsen, A. C., Madsen, K. K., Mori, K., Nynka, M., Fernandez-Perea, M., Pivovaroff, M. J., Ptak, A., Sleator, C., Thornhill, D., Vogel, J. K., Wik, D. R., and Zhang, W. W., "First results from the ground calibration of the NuSTAR flight optics," in [*Space Telescopes and Instrumentation 2011: Ultraviolet to Gamma Ray Optics*], *Proc. SPIE* **8147**, 1111 (2011).

[3] Brejnholt, N., Christensen, F. E., Jakobsen, A. C., Hailey, C. H., Koglin, J. E., Blaedel, K., Stern, M., Thornhill, D., Sleator, C., Zhang, S., Craig, W. W., Madsen, K. K., Decker, T., Pivovaroff, M. J., and Vogel, J. K., "NuSTAR ground calibration: The Rainwater Memorial Calibration Facility (RaMCaF)," in [*Space Telescopes and Instrumentation 2011: Ultraviolet to Gamma Ray Optics*], *Proc. SPIE* **8847**, 1211 (2011).

[4] Christensen, F. E. and Brejnholt, N., "X-ray mirror reflection properties," in [*X-ray Optics*], Ciao, A. B., ed., *Proc. SPIE* **8765**, 716–731 (2003).

[5] Brejnholt, N., Christensen, F. E., Jakobsen, A. C., Hailey, C. H., Koglin, J. E., Blaedel, K., Stern, M., Thornhill, D., Sleator, C., Zhang, S., Craig, W. W., Madsen, K. K., Decker, T., Pivovaroff, M. J., Vogel, J. K., and Westergaard, N. J., "NuSTAR ground calibration II: The effective area," in [*Space Telescopes and Instrumentation 2012: Ultraviolet to Gamma Ray Optics*], *These proceedings* (2012).

[6] Westergaard, N. J., "MT_RAYOR: A versatile raytracing tool for x-ray telescopes," in [*Space Telescopes and Instrumentation 2011: Ultraviolet to Gamma Ray Optics*], *Proc. SPIE* **8847**, 1311 (2011).

[7] Vogel, J. K., Pivovaroff, M. J., Nagarkar, V. V., Kudrolli, H., Madsen, K. K., Koglin, J. E., Hailey, J. E., Craig, W. W., Christensen, F. E., and Brejnholt, N. F., "Application of an EMCCD Camera for Calibration of Hard X-Ray Telescopes," in [*Space Telescopes and Instrumentation 2012: Ultraviolet to Gamma Ray Optics*], *SPIE 8443-93* (2012).

[8] Church, E. L. and Takacs, P. Z., "Specification of surface figure and finish of system performance," *Applied Optics* **32**, 3344–3353 (1993).

[9] Church, E. L. and Takacs, P. Z., "Specification of glancing- and normal-incidence x-ray mirrors," *Optical Engineering* **34**, 353–360 (1995).